

# Vortex structures in the wake of a buoyant tethered cylinder at moderate to high reduced velocities

K. Ryan\*, M.C. Thompson, K. Hourigan

*Fluids Laboratory for Aeronautical and Industrial Research (FLAIR), Department of Mechanical Engineering, Monash University, Clayton, Victoria, 3800, Australia*

Received 17 April 2003; accepted 19 May 2003

## Abstract

Flow-induced vibration of a tethered body immersed in a uniform flow represents a fundamental example of fluid-structure interaction. However, to date little research in this problem has been undertaken. This paper presents results from a two-dimensional numerical simulation of the flow past a tethered circular cylinder with mass ratio,  $m^* = 0.833$ . The Navier–Stokes and dynamic equations of motion of the cylinder are solved using a Galerkin spectral-element/Fourier method. The fluid forces acting on the cylinder, as well as the tension in the tether, are computed and used to determine the resulting cylinder motion. A large peak in the cylinder oscillation is noted for a reduced velocity  $u^* \simeq 19$  corresponding to a negative maximum in the mean lift and a positive maximum in the RMS drag force. Analysis of the vortex structures in the wake of the cylinder, for the cases of  $u^* = 15.4, 19$  and  $21$ , reveal a subtle asymmetry in the shedding process which may provide a mechanism to explain this peak in oscillation amplitude.

© 2003 Elsevier SAS. All rights reserved.

*Keywords:* Vortex-induced vibration; Tethered cylinders

## 1. Introduction

A simple alternative to the problem of a hydro-elastically mounted oscillating cylinder is a cylinder whose motion is confined to an arc by a restraining tether. By considering a wide range of mass ratios,  $m^*$  (the mass of the cylinder divided by the mass of the displaced fluid), we may allow for both positively buoyant bodies ( $m^* < 1$ ) and negatively buoyant bodies ( $m^* > 1$ ), and hence describe a parameter space encompassing a range of practical applications.

The related studies of Williamson et al. [1], Govardhan et al. [2], and Jauvtis et al. [3] deal purely with the interaction of a uniform flow field and a tethered sphere. These experimental studies were performed by placing spheres of various mass ratios and tether lengths into a water channel at various flow speeds. Sustained large peak-to-peak oscillations in the transverse flow-field direction were noted, with amplitudes in the order of two sphere diameters. Small streamwise oscillations of the order of 0.4 sphere diameters were also observed. These results were virtually independent of sphere mass ratio or tether length if they were plotted against the reduced velocity ( $u^* = u/f_n D$ , where  $f_n$  is the natural frequency of the tethered sphere system,  $U$  is the inlet velocity, and  $D$  is the sphere diameter).

This paper provides further results on the mean lift forces as a function of reduced velocity, and analyzes the vortex structures in the wake of a buoyant tethered cylinder extending the recent findings of Ryan et al. [4] and [5]. Ryan et al. [5] have reported on two-dimensional simulations of a tethered circular cylinder in a uniform flow field in the reduced velocity range  $u^* = [1, 25]$  corresponding to a mean layover angle range  $\theta = [0.3^\circ, 83^\circ]$  (see Fig. 1(a)). For reduced velocities in the range  $u^* = [1, 5.5]$ , a

\* Corresponding author.

*E-mail address:* [Kris.Ryan@eng.monash.edu.au](mailto:Kris.Ryan@eng.monash.edu.au) (K. Ryan).

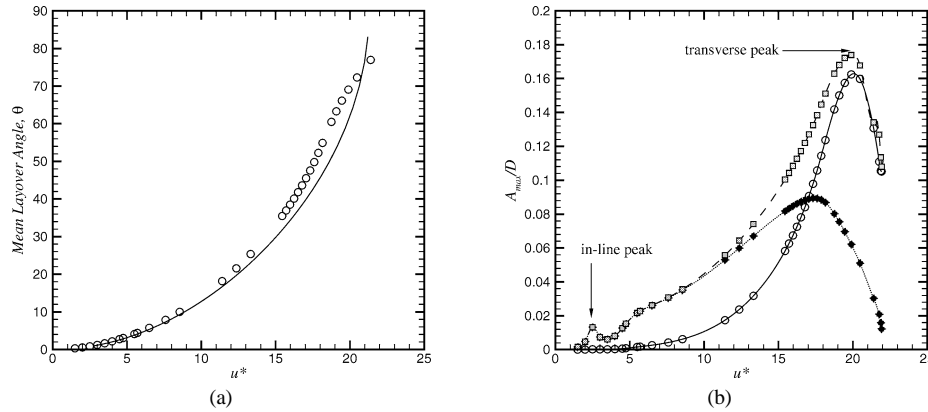


Fig. 1. (a) Mean layover angle as a function of reduced velocity.  $\circ$  numerical results, — analytical estimate (note the analytical estimate is made using Eq. (8) and assumes a fixed  $C_D = 1.34$ , which is equivalent to the drag coefficient for a fixed cylinder at  $Re = 200$ ). (b) Normalized amplitude of oscillation as a function of reduced velocity;  $\blacklozenge$  in-line component of normalized oscillation amplitude,  $\circ$ , transverse component of normalized oscillation amplitude,  $\square$  normalized oscillation amplitude in the direction of motion.

change in the drag frequency was noted, such that for  $u^* \gtrsim 3.5$  the drag and lift have the same frequency and are in phase. This change was due to the in-line component of the cylinder motion reducing the pressure at the stagnation point as the cylinder moved in the downstream direction, to the extent that the drag force is dominated by the cylinder oscillation frequency, which is equal to the lift frequency. A local peak in the amplitude of oscillation was noted to occur at  $u^* \simeq 19$  (see Fig. 1(b)) with a corresponding peak in the in-line force coefficient, and energy transfer from the fluid to the cylinder motion; however the reason why this peak should exist has yet to be explained.

As described by Ryan et al. [5], at large layover angles (high reduced velocities), the tethered cylinder motion is dominated by the transverse component and oscillates in a fashion similar to a low mass-damped hydro-elastically mounted cylinder. Govardhan and Williamson [6] found three branches of flow-induced oscillation for a low mass-damped hydro-elastically mounted cylinder; the initial, upper and lower branches. The upper branch was found to have considerably greater oscillation amplitudes than either of the other two branches. The reduced velocity range where upper branch cylinder oscillations occurred was found to vary inversely with the mass ratio of the cylinder. Further work by Govardhan and Williamson [7] found that the upper branch was sustained up to an infinite reduced velocity for  $m^* < 0.54$ .

This investigation presents two-dimensional simulations for flow past a buoyant tethered cylinder in the reduced velocity range,  $u^* = [1, 25]$ . High amplitude oscillations were noted for  $u^* \simeq 19$  in agreement with the findings of Ryan et al. [5]. At higher reduced velocities, the amplitude of oscillation reduces significantly in agreement with the findings for the hydro-elastically mounted cylinder.

The study by Ryan et al. [5] did not specifically concentrate on the mechanisms causing the large peak in the oscillation amplitude at  $u^* \simeq 19$  nor did they report a negative mean lift. The mean forces acting on the tethered cylinder are reported in this paper, along with the mean flow field and snapshots of the vortex shedding structures in the wake of the tethered cylinder for  $u^* = 15.4, 19$  and  $21$  at the top and bottom of the oscillation cycle.

## 2. Problem formulation

The coordinate system and geometry of the problem are shown in Fig. 2(a). Note that  $\theta$  is the mean layover angle taken from the vertical ( $y$ ) axis, and  $\phi$  is the instantaneous angle of oscillation about  $\theta$ . The fluid forces acting on the tethered body are composed of Drag ( $F_D$ ), Lift ( $F_L$ ), and Buoyancy ( $B$ ) terms. A restoring tension force ( $T$ ) in the tether is also present. The problem is fully described in two dimensions by the coupled system of the incompressible Navier–Stokes equations (Eqs. (1a) and (1b)) and the equations of motion describing the body acceleration in response to calculated fluid forces (Eqs. (2a) and (2b)). The Navier–Stokes equations are

$$\frac{\partial \mathbf{u}'}{\partial t} + (\mathbf{u}' \cdot \nabla \mathbf{u}') \mathbf{u}' = -\frac{1}{\rho_f} \cdot \nabla' + \frac{1}{Re} \nabla'^2 \mathbf{u}', \quad (1a)$$

$$\nabla' \cdot \mathbf{u}' = 0, \quad (1b)$$

where  $\mathbf{u}'$  is the velocity field and  $p'$  is the pressure field. The equations describing the body motion are given by

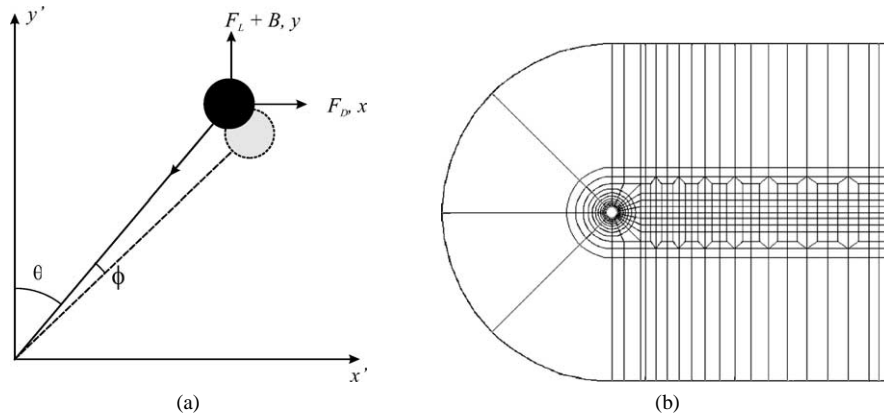


Fig. 2. (a) Idealized schematic of the tethered cylinder in fluid flow. The tethered cylinder has a mean layover angle from the vertical,  $\theta$ , and a oscillation angle about this mean layover angle,  $\phi$ . (b) Macro element mesh used for the simulations.

$$\ddot{x} = \frac{F_x}{m} = \frac{\gamma}{L^2 m^*} \left[ (L^2 - x^2) C_D - xy \left( C_L + (1 - m^*) \left( \frac{\pi}{2Fr^2} \right) \right) \right], \quad (2a)$$

$$\ddot{y} = \frac{F_y}{m} = \frac{\gamma}{L^2 m^*} \left[ (L^2 - y^2) \left( C_L + (1 - m^*) \left( \frac{\pi}{2Fr^2} \right) \right) - xy C_D \right], \quad (2b)$$

where  $Fr = U/\sqrt{gD}$  is the Froude number,  $L$  is the tether length, and  $\gamma = 2u^2/(\pi D)$ . Note that  $\gamma$  is dimensional and has units of acceleration. More details of the equations of motion, including the derivation of Eqs. (2a) and (2b) are provided in Ryan et al. [5]. The controlling parameter in Eqs. (2a) and (2b) is the Froude number. Experimentally, the Froude number is varied by altering the inlet velocity. This has the added effect of changing the Reynolds number, which directly affects the development of the vortex structures in the near wake region. Numerically, the reduced velocity and Froude number may be altered independently of the Reynolds number. For the results presented in this paper, the Reynolds number was held fixed at  $Re = 200$  for all simulations. This value was chosen in order to simulate as closely as possible a range of experimental conditions, as both the drag coefficient and vortex shedding frequency may be considered reasonably constant for the range  $200 < Re < 10^5$ . At higher Reynolds numbers, two-dimensional simulations have a higher Strouhal number and an excessively short formation region relative to experimental results and three-dimensional direct numerical simulations.

In order to compare with previous experimental research and vortex-induced vibration results for other bodies (notably Williamson and Govardhan [1] and Govardhan and Williamson [6]), the findings are presented against the reduced velocity,  $u^*$ , which following the work of Ryan et al. [5], is defined as

$$u^* = \frac{U}{f_n D} = \frac{2\pi}{\sqrt{2}} \left( \frac{(m^* + C_A)L^*}{(C_D^2 + [\alpha(1 - m^*)])^{1/2}} \right)^{1/2}, \quad (3)$$

where  $f_n$  is the natural frequency of the tethered cylinder system,  $C_A$  is the added mass coefficient (for a circular cylinder,  $C_A = 1$ ),  $C_D$  is the mean drag coefficient, and  $L^* = L/D$  is the normalized tether length.

In this investigation, a fixed tether length of  $L^* = 5.05$  and mass ratio of  $m^* = 0.833$  were chosen to provide direct comparisons with the previous findings of Ryan et al. [5]. Simulations were performed over the reduced velocity range  $u^* = [1, 25]$ .

### 3. Numerical method

For all simulations the mesh is held fixed to the cylinder and the Cartesian coordinate reference frame is transformed to a non-inertial reference frame attached to the body with the following transformation:

$$\mathbf{x}' = \mathbf{x} - \mathbf{X}(t), \quad (4)$$

where  $\mathbf{x}'$  is position vector relative to the accelerating reference frame, and  $\mathbf{X}(t)$  is the displacement of the cylinder and is described in terms of  $\theta + \phi$  as:

$$X(t) = L \cos(\theta + \phi(t)), \quad Y(t) = L \sin(\theta + \phi(t)). \quad (5)$$

In the transformed system of coordinates, the cylinder appears stationary, although it is allowed to rotate about the fixed tether point. Given the transformation (4), the Navier–Stokes and continuity Eqs. (1a) and (1b) become:

$$\frac{\partial \mathbf{u}'}{\partial t} + (\mathbf{u}' \cdot \nabla) \mathbf{u}' = -\frac{1}{\rho_f} \nabla p + \frac{1}{Re} \nabla^2 \mathbf{u}' + \mathbf{A}(\mathbf{u}, p, \mathbf{X}), \quad (6)$$

$$\nabla \cdot \mathbf{u}' = 0, \quad (7)$$

where the forcing term  $\mathbf{A}(\mathbf{u}, p, \mathbf{X})$  is an additional acceleration introduced by the coordinate transformation, Eq. (4), and is the acceleration of the cylinder given by Eqs. (2a) and (2b). Due to the attachment of the coordinate system to the cylinder, the cylinder will rotate as it moves about the base pivot. Hence, the boundary conditions need to be altered in order to account for this effect.

The equations of motion for the fluid and the cylinder are discretized in space using a spectral-element method. Typically, eighth-order Lagrangian polynomials were used as the tensor-product expansion basis. Eqs. (2a) and (2b), governing the body's motion, are solved using a predictor-corrector technique. The Navier–Stokes and continuity equations (2a) and (2b) are discretized in time using a three-step time-splitting approach (see Karniadakis et al. [8] for further details). The acceleration term  $\mathbf{A}$  is combined with the non-linear terms and these are treated in the first sub-step of the time update.

The coupled fluid/structure equations are solved in three steps. First, an initial angle  $\theta$  is set (corresponding to an initial displacement  $\mathbf{x}_0$ ) and the fluid equations are solved. The fluid forces acting on the cylinder are then calculated and the structure's motion is updated using Eqs. (2a) and (2b) and the process repeated.

Detailed resolution tests were performed on a stationary cylinder to verify grid independence. A Reynolds number of  $Re = 500$  was chosen for two reasons; first it represents the highest Reynolds number considered for this (and other) investigations and therefore represents the most rigorous grid resolution study possible; second our present grid resolution study may be directly compared with the grid resolution study of Blackburn and Henderson [9] (however, as noted, simulations presented in this paper are for  $Re = 200$ ). The order of the interpolating polynomials was varied between from  $N = 5$  to  $N = 9$ . Flow quantities such as the Strouhal number, lift and drag coefficients were measured and compared. The results are summarized in Table 1. For all measures employed, the variation between the values at  $N = 7$  and  $N = 9$  is less than 1%. Furthermore, the values of all measures for  $N = 8$  (used in all simulations) compare to within 1% of the numerical values of Blackburn and Henderson [9], and Henderson [10]. Mesh independence was also verified for the moving cylinder by considering the two extremes of tether angle. At small angles, motion was predominantly in the cross-flow direction, whereas at large angles, the motion was largely in the stream-wise direction. For each value of  $N$  from  $5 \leq N \leq 10$ , mean tether angles, oscillation amplitudes, oscillation frequencies and drag and lift coefficients were measured for these two extreme cases. Again, all quantities compare to within 1% for the  $N = 8$  case. A plot of the two-dimensional mesh showing only the macro elements is shown in Fig. 2(b).

Table 1

Convergence results for a stationary cylinder. The symbol ( $p$ ) denotes peak values, ( $m$ ) denotes mean values

N	5	6	7	8	9
$C_L(p)$	1.1873	1.1809	1.1817	1.1818	1.1822
$C_D(p)$	1.5897	1.5792	1.5798	1.5793	1.5795
$C_D(m)$	1.4561	1.4457	1.4462	1.4461	1.4459
$St$	0.2270	0.2264	0.2267	0.2267	0.2267

Table 2

Position of positive and negative vortex cores downstream of the cylinder, formation length, and wake thickness  $2\delta$ , where  $\delta$  is the boundary layer thickness measured at the core position

	$u^* = 15.4$	$u^* = 19$	$u^* = 21$
$Core^+$	0.615	0.594	1.038
$Core^-$	0.415	0.532	1.038
Formation length	1.188	1.030	1.770
Wake thickness	1.688	1.656	1.788

4. Results

For any given reduced velocity, the cylinder oscillations may be decomposed into the transverse component and the inline component. Increasing the reduced velocity consequently increases the cylinder mean layover angle,  $\theta$ , which may be determined from the ratio of mean drag force to buoyancy force and is given in non-dimensional form as:

$$\theta = \tan^{-1} \left( \frac{2\overline{C_D}Fr^2}{\pi(1-m^*)} \right). \tag{8}$$

When the mean layover angle exceeds  $45^\circ$ , the cylinder oscillations begin to be dominated by the transverse component. At very large layover angles ( $\theta > 70^\circ$ ), the transverse component of oscillation is significantly larger than the inline component and the cylinder should oscillate similarly to a low mass-damped hydro-elastically mounted cylinder.

For the given cylinder mass ratio and tether length studied ( $m^* = 0.833$ ,  $L^* = 5.05$ ), as the reduced velocity is increased from  $u^* = 5$  to  $u^* = 19$ , a local maximum in the cylinder displacement amplitude is observed (see Fig. 1(b)). As the reduced velocity is increased further, the amplitude decreases markedly, indicating a sudden change in the fluid-body interaction.

Section 4.1 presents new results of the mean lift acting on the cylinder as a function of reduced velocity. Mean vortex fields for  $u^* = 15.4, 19$  and  $21$  are also presented. The mean vortex profile is seen to change considerably with reduced velocity. The mean position of the centroid of the shedding vortex and the formation length is determined for each reduced velocity. These findings allow us to relate changes in the RMS drag and lift forces acting on the cylinder to the local maximum found in the amplitude of oscillation for  $u^* = 19$ .

The hydrodynamic forces acting on a body may be inferred directly from analysis of the vortex structures in the vicinity of the body. By analyzing the size and intensity of the vortices, and their distance to the surface of the body, the hydrodynamic forces acting on the body may be determined.

A qualitative description of the tethered cylinder interaction with the vortex structures in the wake flow field over a period of oscillation is presented in Section 4.2 for  $u^* = 15.4, 19$  and  $21$ . From this description two branches of cylinder oscillation are identified; the first (referred to as the transition branch) is found for both  $u^* = 15.4$  and  $19$ , and from Fig. 1(b) appears to occur in the reduced velocity range  $u^* = 5$  to  $19$  for this particular cylinder mass ratio and tether length ratio. The second branch occurs for  $u^* > 19$  and (for the case of  $u^* = 21$ ) appears similar to the ‘lower branch’ of shedding for a low mass-damped hydro-elastically mounted cylinder (as described by Govardhan and Williamson [6]).

4.1. Mean lift and vorticity Fields

The mean lift, plotted both as a function of reduced velocity and mean layover angle, is presented in Fig. 3. For a large range of the reduced velocities investigated, a net negative lift was observed, indicating an asymmetry in the mean wakes about the centreline. Analysis of Figs. 4(a)–(c), indicates a distinct asymmetry in the wake for  $u^* = 15.4$  and  $19$ . The wake formation region for these reduced velocities is significantly shorter than for  $u^* = 21$ . Here, the formation length is measured as the distance from the mean position of the rear surface of the cylinder to the furthest downstream location of vorticity,  $|\omega_z| \geq 1.0$ . The values of the formation length are detailed in Table 1. Both these effects are due to the asymmetric forces imposed by the motion of the cylinder during the shedding cycle.

A difference in the downstream extent of vortex *A* compared to vortex *B* is observed for both  $u^* = 15.4$  and  $19$ . This difference appears to reduce with increasing reduced velocity. It is speculated that this is due to the reduction in the inline component of oscillation as the reduced-velocity is increased.

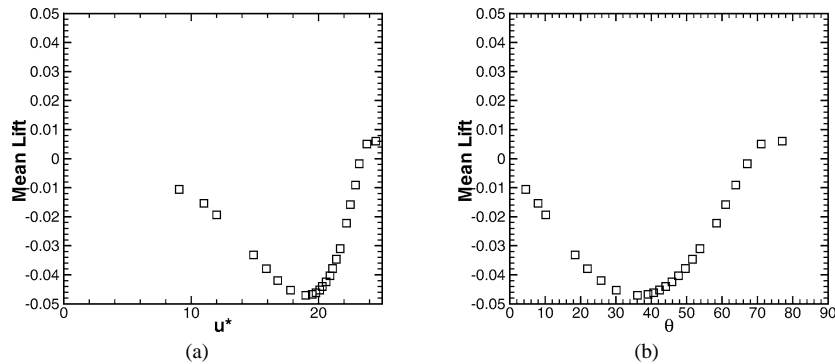


Fig. 3. Mean lift as a function of (a) reduced velocity and (b) mean layover angle.

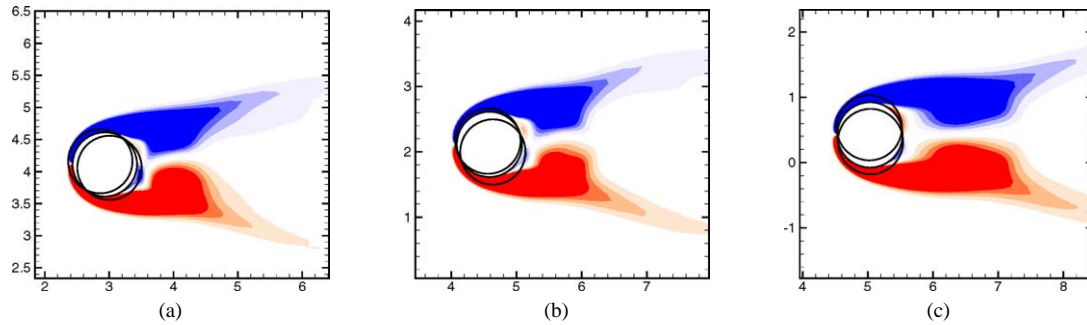


Fig. 4. Contours of the mean span-wise vorticity in the wake of a tethered cylinder for (a)  $u^* = 15.4$ , (b)  $u^* = 19$ , and (c)  $u^* = 21$ .

For  $u^* = 15.4$  and  $19$ , the centroid of the shedding vortex structure is  $0.6$  diameters downstream of the mean position of the rear surface of the cylinder. As the reduced-velocity is increased to  $u^* = 21$ , the centroid of the shedding vortex cores increases to  $1.05$  cylinder diameters downstream of the mean position of the rear surface of the cylinder. From the findings of Bearman [11], it would be anticipated that the mean drag acting on the cylinder would therefore decrease as the reduced-velocity is increased from  $u^* = 19$  to  $u^* = 21$ .

#### 4.2. Vorticity time series

Figs. 5, 6 and 7 show contours of vorticity at the top and bottom of the oscillation cycle for  $u^* = 15.4$ ,  $19$  and  $21$  respectively. These reduced velocity values are considered as they fall in the vicinity of the transverse peak shown in Fig. 1(b) above; the case of  $u^* = 19$  has the largest amplitude oscillations found for the reduced-velocity range investigated ( $u^* = [1, 25]$ ). For each

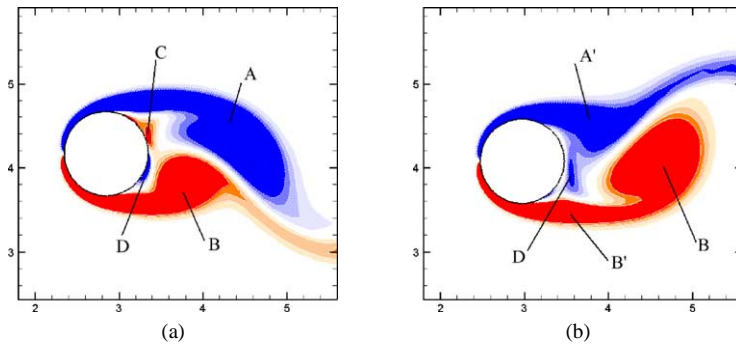


Fig. 5. Contours of span-wise vorticity in the wake of a tethered cylinder for  $u^* = 15.4$ ; (a) corresponds to the top of the cycle, (b) corresponds to the bottom of the oscillation cycle. The flow is from left to right.

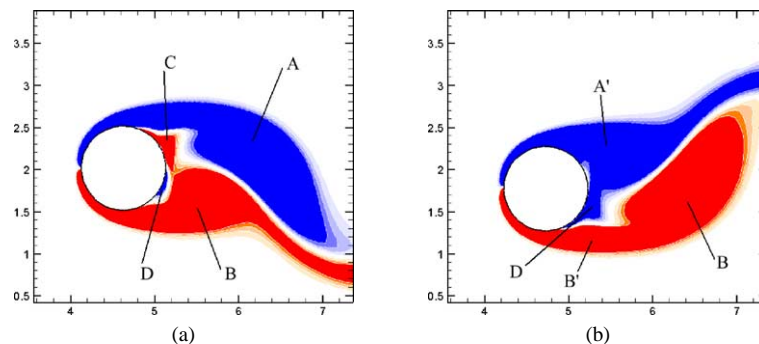


Fig. 6. Contours of span-wise vorticity in the wake of a tethered cylinder for  $u^* = 19$ ; (a) corresponds to the top of the cycle, (b) corresponds to the bottom of the oscillation cycle. The flow is from left to right.

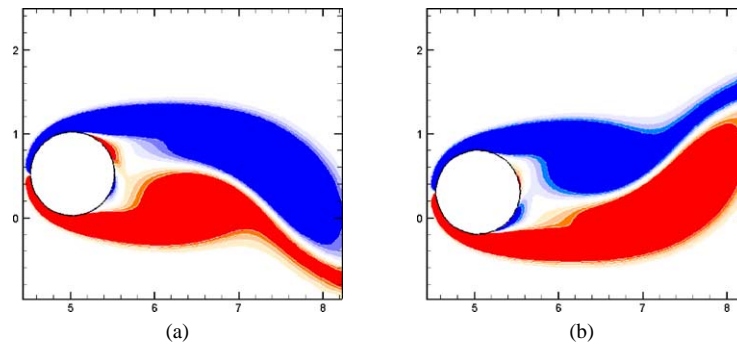


Fig. 7. Contours of span-wise vortex structures in the wake of a tethered cylinder for  $u^* = 19$ , (a) corresponds to the top of the cycle, (b) corresponds to the bottom of the oscillation cycle, the flow is from left to right.

reduced-velocity, the first frame (frame a) coincides with the most counter-clockwise position of the cylinder (referred to as the top of the oscillation cycle), and the second frame (frame b) coincides with the bottom of the oscillation cycle.

As there is no external damping term in the equations of motion (Eqs. (2a) and (2b)), and an appreciable amplitude in the reduced velocity range investigated, the phase lag between the force acting on the cylinder and the resultant displacement is  $180^\circ$ . Therefore, for each reduced velocity, the first frame (frame a) coincides with the maximum positive peak in the fluctuating fluid forces acting on the cylinder.

Fig. 5 shows contours of vorticity ( $\omega_z$ ) for the reduced-velocity,  $u^* = 15.4$ . At this reduced-velocity, the mean layover angle  $\theta = 35.5^\circ$  and the oscillations are dominated by the inline component (see Figs. 1 (a) and (b)). At the top of the cylinder oscillation cycle (Fig. 5(a)) four vortex structures are observed. Two of these vortices (labelled *A* and *B*) represent the shedding negative and positive vortex structures respectively. In response to the pressure gradient induced by the presence of both vortices *A* and *B*, and the no-slip condition on the surface of the cylinder, two secondary vortices (labelled *C* and *D*, representing positive and negative vortex structures, respectively) are found in the vicinity of the rear surface of the cylinder. Fig. 5(a) represents a positive peak in the fluctuating hydrodynamic forces acting in the direction of cylinder motion; the combined effect of the size and location of vortex *A* and vortex *B* directly behind the cylinder induce a low pressure region. In Fig. 5(b), the cylinder is once again momentarily stationary (now located at the bottom of the oscillation cycle), the fluctuating fluid forces acting on the cylinder have reached a maximum negative value. Comparing the flow field at the top and bottom of the cycle, a subtle asymmetry in the wake is noted. At the top of the cycle, vortex *A* is far more elongated than vortex *B* at the bottom of the cycle. The asymmetry is also apparent when observing Fig. 5(b) where vortex *D* is observed to dominate the entire near wake region.

As the reduced-velocity is increased to  $u^* = 19$  (Fig. 6) representing the largest amplitude oscillations over the range of reduced velocities studied ( $u^* = [1, 25]$ ), the cylinder wake structure is very similar to the case of  $u^* = 15.4$  at every stage of the oscillation cycle, indicating that the mode of cylinder oscillation is similar. At this reduced velocity, the mean layover angle has increased to  $\theta = 63.3^\circ$  and the cylinder oscillation is now dominated by the transverse component. The vortex structures have increased significantly in size, this occurs for two reasons. First, as the reduced-velocity is increased, the period of oscillation also increases and the vortex structures have more time to develop over an oscillation cycle. Second, at this particular reduced velocity ( $u^* = 19$ ) the amplitude of oscillation of the cylinder is significantly greater than for the case of  $u^* = 15.4$ . This is also associated with an increase in the fluctuating acceleration acting on the cylinder, which increases the size of the vortices being shed from the cylinder. It is assumed that the increase in oscillation amplitude is due to the increase in the Froude number, with a subsequent reduction in the mean vertical force ( $\overline{F_y}$ ) which results in the mean layover angle increasing and the cylinder oscillation being less constrained by the inline component.

As the reduced velocity is further increased to  $u^* = 21$ , there is a significant change in the wake structure, as compared to the two previous cases. Here the mean layover angle  $\theta = 83^\circ$  and the motion is dominated by the transverse component. At this reduced velocity, the inline component of the oscillation amplitude is  $x_{\text{amp}} \simeq 0.012D$ , whereas the transverse component of the oscillation amplitude is  $y_{\text{amp}} \simeq 0.1D$ . The near wake structure (comprising vortex *C* and *D*) is considerably more symmetric.

In summary, a mode of wake formation has been identified (and will be referred to as the ‘transition mode’) from the vortex structures in the wake of the oscillating cylinder for  $u^* = 15.4$  and 19. From the findings of Ryan et al. [5], for this cylinder mass ratio and tether length ratio, the transition mode would appear to exist over the range  $u^* = [5, 19]$  and involves a transition from cylinder oscillations dominated by the inline component (at low reduced velocities) to oscillations dominated by the transverse component (at high reduced velocities).

In the transition mode, the inline motion of the cylinder appears to be critical to the vortex shedding structures in the wake, and produces a subtle but distinct asymmetry in the shedding wake not observed for the flow past a freely oscillating cylinder (see Govardhan and Williamson [6]). The inline component of motion acts to reduce the length of the formation region, inducing

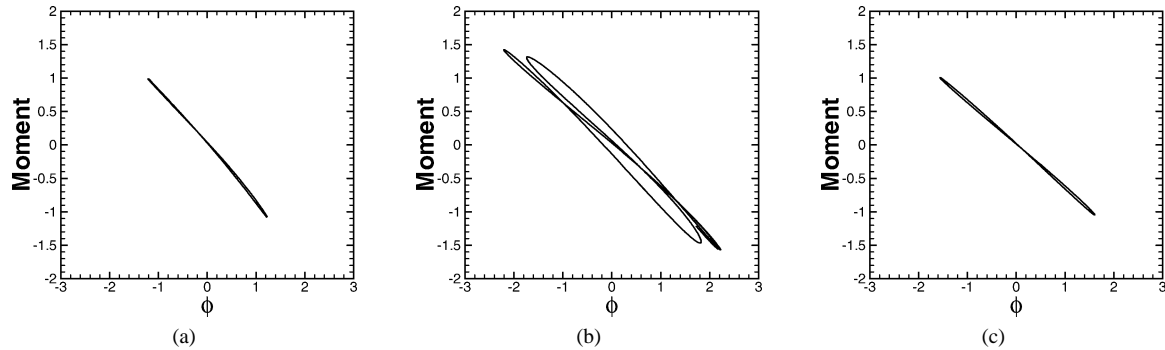


Fig. 8. Cylinder displacement  $\phi$  as a function of the normalized moment acting on the tethered cylinder system, for the reduced velocities; (a)  $u^* = 15.4$ ; (b)  $u^* = 19$ ; and (c)  $u^* = 21$ . Each limit cycle is traversed in a clock-wise direction.

larger forces in both the inline and transverse directions to act on the cylinder. As the mean layover angle,  $\theta$ , exceeds  $45^\circ$ , the oscillations are increasingly dominated by the transverse component, and the inline component of oscillation rapidly diminishes.

As the reduced-velocity is increased from  $u^* = 15.4$  to  $u^* = 19$ , the transverse oscillations of the cylinder are less constrained by the resultant inline oscillations. The overall effect is an increase in the amplitude of cylinder oscillation as the reduced-velocity is increased to  $u^* = 19$ .

As the reduced-velocity is further increased to  $u^* = 21$ , the inline component of oscillation is not sufficient to maintain the transition mode. The shed vortices are now free to convect away from the cylinder and the length of the formation region increases. The forces acting on the cylinder diminish and the amplitude of oscillation decreases markedly, in agreement with the findings of Bearman [11]. The cylinder is now oscillating in a fashion similar to a low mass-damped hydro-elastically mounted cylinder oscillating in the lower branch of oscillation (as described by Govardhan and Williamson [6]).

To quantitatively compare the force acting on the cylinder as a function of its relative position, the limit cycles of the cylinder position ( $\phi$ ) as a function of the normalized moment acting on the tethered cylinder system ( $M$ ) for the three values of  $u^*$  investigated above are presented in Fig. 8.

For each reduced velocity, the moment (and hence the force acting on the cylinder) is clearly  $180^\circ$  out of phase with the cylinder position,  $\phi$ , hence the maximum value of  $\phi$  coincides with the minimum value of  $M$  and vice versa.

For  $u^* = 15.4$  asymmetry in the Moment acting on the cylinder when comparing the top and bottom of the cycle. This asymmetry is considerably amplified for  $u^* = 19$ . For  $u^* = 21$  the oscillation cycle is clearly more symmetric. As each cycle in Fig. 8 form a closed limit cycle, the mean forces acting on the cylinder in the direction of motion must equate to zero over one cycle, and the cylinder will therefore oscillate about the mean angle  $\theta$ .

## 5. Conclusion

Two-dimensional numerical simulations of the flow past a tethered cylinder with mass ratio  $m^* = 0.833$  have been performed. The Navier–Stokes and dynamic equations of motion of the cylinder are solved using a spectral element method. The fluid forces acting on the cylinder, as well as the tension in the tether, are computed and used to determine the resulting cylinder motion. A large peak in the cylinder oscillation was noted for a reduced-velocity  $u^* \simeq 19$ . Analysis of the vortex structures in the wake of the cylinder, for the case of  $u^* = 15.4$ , reveals that the inline motion of the body in the reduced-velocity range  $u^* = [5, 19]$  reduces the length of the formation region, and increases the forces acting on the cylinder. As the reduced-velocity is increased to  $u^* = 19$ , the change in the mean layover angle allows a greater transverse amplitude of oscillation for a given inline amplitude, and hence the overall amplitude of oscillation is increased. For both these reduced velocities, the near wake, and the moment acting on the cylinder over one period, are observed to be asymmetric. As the reduced-velocity is further increased to  $u^* = 21$ , there is insufficient inline motion to enable enhanced interaction with the wake vortex structures, and the formation length increases markedly.

## Acknowledgements

Kris Ryan would like to acknowledge support provided through a Monash Departmental Scholarship. The authors would like to acknowledge strong support from the Victorian Partnership for Advanced Computing, the Australian Partnership for Advanced Computing, and a large grant from the Australian Research Council (ARC), which enabled this research to take place.

**References**

- [1] C. Williamson, R. Govardhan, Dynamics and forcing of a tethered sphere in a fluid flow, *J. Fluids Structures* 11 (1997) 293–305.
- [2] R. Govardhan, C. Williamson, Vortex-induced motions of a tethered sphere, *J. Wind Engrg.* 69–71 (1997) 375–385.
- [3] N. Jauvtis, R. Govardhan, C. Williamson, Multiple modes of vortex-induced vibration of a sphere, *J. Fluids Structures* 15 (2001) 555–563.
- [4] K. Ryan, M. Thompson, K. Hourigan, Energy transfer in a vortex induced vibrating tethered cylinder system, in: *Conference on Bluff Body Wakes and Vortex-Induced Vibrations (BBVIV3)*, Port Douglas, 17th–20th December, 2002, pp. 57–60.
- [5] K. Ryan, C. Pregalato, M. Thompson, K. Hourigan, Flow-induced vibrations of a tethered circular cylinder, *J. Fluids Structures*, in press.
- [6] R. Govardhan, C. Williamson, Modes of vortex formation and frequency response of a freely vibrating cylinder, *J. Fluid Mech.* 420 (2000) 85–130.
- [7] R. Govardhan, C. Williamson, Resonance forever: existence of a critical mass and an infinite regime of resonance in vortex-induced vibration, *J. Fluid Mech.* 473 (2003) 147–166.
- [8] G. Karniadakis, M. Israeli, S. Orszag, High-order splitting methods of the incompressible navier-stokes equations, *J. Comput. Phys.* 97 (1991) 414–443.
- [9] H.M. Blackburn, R.D. Henderson, A study of two-dimensional flow past an oscillating cylinder, *J. Fluid Mech.* 385 (1999) 255–286.
- [10] R. Henderson, Details of the drag curve near the onset of vortex shedding, *Phys. Fluids* 7 (1995) 2102–2104.
- [11] P. Bearman, Investigation of the flow behind a two-dimensional model with a blunt trailing edge and fitted with splitter plates, *J. Fluid Mech.* 21 (1965) 241–255.